

# Geophysical Research Letters

## RESEARCH LETTER

10.1029/2020GL089108

### Key Points:

- Persistent long-period (25 and 18 s) seismic signals appear in ambient noise cross-correlations of OBS data in the western-central Pacific
- The signals are originated from Ambrym volcano in the Vanuatu Arc
- Source locations of the two signals may be different, but both are possibly located at shallow depths right beneath the active cones

### Supporting Information:

- Supporting Information S1

### Correspondence to:

Y. Kawano,  
ykawano@eri.u-tokyo.ac.jp

### Citation:













Kawano, Y., Isse, T., Takeo, A., Kawakatsu, H., Suetsugu, D., Shiobara, H., et al. (2020). Persistent long-period signals recorded by an OBS array in the western-central Pacific: Activity of Ambrym volcano in Vanuatu. *Geophysical Research Letters*, 47, e2020GL089108. <https://doi.org/10.1029/2020GL089108>

Received 2 JUN 2020

Accepted 11 SEP 2020

Accepted article online 14 SEP 2020

## Persistent Long-Period Signals Recorded by an OBS Array in the Western-Central Pacific: Activity of Ambrym Volcano in Vanuatu

Yuki Kawano<sup>1</sup> , Takehi Isse<sup>1</sup> , Akiko Takeo<sup>1</sup> , Hitoshi Kawakatsu<sup>1</sup> , Daisuke Suetsugu<sup>2</sup> , Hajime Shiobara<sup>1</sup> , Hiroko Sugioka<sup>3</sup> , Aki Ito<sup>2</sup> , Yasushi Ishihara<sup>2</sup>, Satoru Tanaka<sup>2</sup> , Masayuki Obayashi<sup>2</sup> , Takashi Tonegawa<sup>2</sup> , and Junko Yoshimitsu<sup>2</sup> 

<sup>1</sup>Earthquake Research Institute, The University of Tokyo, Tokyo, Japan, <sup>2</sup>Japan Agency for Marine-Earth Science and Technology, Kanagawa, Japan, <sup>3</sup>Graduate School of Science, Kobe University, Hyogo, Japan

**Abstract** Strong long-period seismic signals at periods around 25 and 18 s appear in the ambient noise cross-correlation functions recorded by an array of ocean bottom seismometers (OBSs) in the western-central Pacific. The signal amplitude varies from time to time, and the apparent travel times of the signals are typically smaller than those expected for the Rayleigh waves propagating along the great circle connecting the station pairs. From the cross-correlation functions, the signal sources are located in the Vanuatu Arc. Local data analysis suggests the signals originate from two different sources possibly located at depths of ~0–1 km below the sea level beneath the active cones of Ambrym volcano.

**Plain Language Summary** Spatially localized sources that persistently generate long-period seismic waves at periods longer than 10 s are reported worldwide. For some sources, the excitation mechanisms have been well-investigated. A volcano in Japan generates such waves that travel more than thousands of kilometers. For others, however, the excitation origins are still poorly understood. These include the one observed in the Vanuatu Arc. A temporal observation network of seismometers installed on the seafloor in the western-central Pacific observed persistent waves peaking at around two different periods. From the data analysis, we find the signals originate from an active volcano, Ambrym volcano, in the Vanuatu Arc. Besides, we find that those seismic waves are most likely originated from two different sources possibly located at shallow depths beneath the volcano.

## 1. Introduction

The ambient noise cross-correlation function (NCF) is useful to investigate the crustal and uppermost mantle seismic structure beneath continents, island arcs, and the ocean (e.g., Nishida et al., 2008; Shapiro et al., 2005; Takeo et al., 2013). Since the analysis typically assumes homogeneously and randomly distributed noise source around stations, the existence of a spatially localized source that persistently generates seismic waves, such as a volcano, may bias the surface wave dispersion measurements essential for the structure research (e.g., Shapiro et al., 2006). For example, Aso volcano in Japan has been known to generate persistent long-period tremors dominant in a period range of 3–15 s that had been observed locally and regionally (e.g., Kaneshima et al., 1996; Kawakatsu et al., 1994, 2000) that are recently observed by stations in East Asia via NCFs (Zeng & Ni, 2010, 2011).

One of the well-known localized signal sources is in the Gulf of Guinea that generates 26 s signal (Holcomb, 1980, 1998; Oliver, 1962, 1963; Xia et al., 2013; Xia & Chen, 2020). Shapiro et al. (2006) reported that the signal resulted in fast-arriving wave trains in NCFs computed for the North American and European stations. NCFs observed in East Asia and the western Pacific also show the existence of fast-arriving signals centered around 26 s (Shapiro et al., 2006), but more recently Zeng and Ni (2014) suggested that this signal was independent from that of the Gulf of Guinea and originated from one of the volcanoes in the Vanuatu Arc region. Until now, however, the exact source origins and the excitation mechanisms of the signals originated from the Gulf of Guinea and the Vanuatu Arc are still poorly understood. These far-reaching persistent signals require continuous input of energy, thus featuring very unique processes inside the Earth, and the elucidation of their source processes in detail may bring new ways to utilize the ambient noise cross-correlation functions.

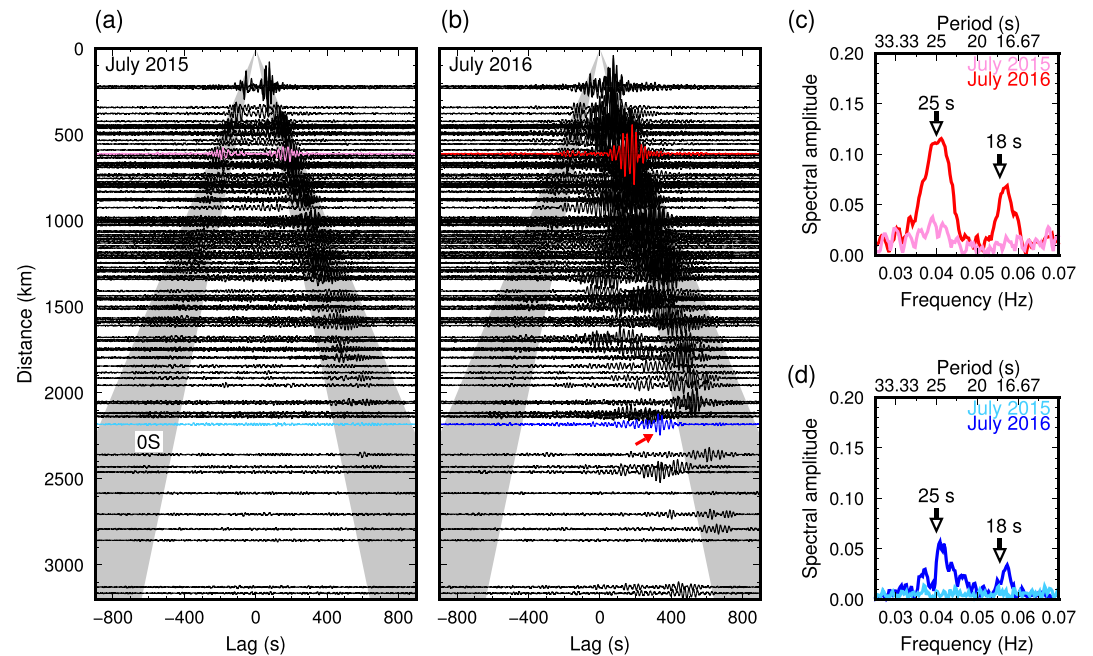


**Figure 1.** Examples of the NCFs of vertical component seismograms recorded by the OJP array (Figure 2a). NCFs are computed from 1-month records and band-pass filtered between 0.025 and 0.070 Hz. (a, b) NCFs for July 2015 and July 2016 (only for BBOBS pairs are shown): They are displayed such that the positive lag time corresponds to waves traveling away from the inferred source locations in the Vanuatu Arc (Figure 2b). The gray-shaded bands indicate the time interval corresponding to a group velocity window of 2.5–5.0 km/s when interstation fundamental-mode Rayleigh waves (0S) are expected to arrive. The red arrow points a fast arriving signal. (c, d) The Fourier amplitude spectra of the NCFs highlighted in (a) and (b) with the same colors. Black arrows indicate positions of 25 and 18 s.

From December 2014 to January 2017, a geophysical network was deployed around the Ontong Java Plateau (OJP). This network, the OJP array, includes 23 broadband ocean bottom seismometers (BBOBSs) together with broadband seismic stations at two nearby islands and is designed to reveal the seismic structure of the Plateau (Suetsugu et al., 2018). During the process of conducting the Rayleigh wave dispersion analysis for regional tomography (Kawano et al., 2019), we noticed, in NCFs, the presence of band-limited signals whose apparent travel time is smaller than that of interstation Rayleigh waves, suggesting the existence of persistent spatially localized signal sources. In this paper, based on the analysis of NCFs of the OJP array data, supplemented by regional and local data, we show conclusively that the signals are emitted from an active volcano, Ambrym in the Vanuatu Arc, and discuss the excitation origin in association with the subsurface magma system therein.

## 2. Analysis of Persistent Long-Period Signals

### 2.1. OJP Array Data

The NCFs at the OJP array are computed from vertical component seismograms. We first perform tilt-noise reduction from the BBOBS data (Bell et al., 2015; Crawford & Webb, 2000). After dividing whole seismograms into 2,000-s-long sections with a 50% overlap, we discard any sections containing glitches or earthquake-generated signals. Then we stack all the Fourier-transformed sections with spectral whitening (Bensen et al., 2007) and obtain NCFs via the inverse Fourier-transform. The NCFs for July 2015 (Figure 1a) and for July 2016 (Figure 1b) show a difference in the signal appearance: In July 2015, the NCFs show clearly the propagation of interstation fundamental-mode Rayleigh waves (0S in Figure 1a), whereas, in July 2016, some signals arrive earlier than 0S, and the amplitudes of the fast-arriving signals are larger compared to those of 0S observed in July 2015 (Figures 1a and 1b). The NCFs for July 2016 show significant peaks centered around 25 s (0.040 Hz) and 18 s (0.057 Hz) in spectra, whereas the NCFs for July 2015 show less significant peaks at those periods (Figures 1c and 1d).

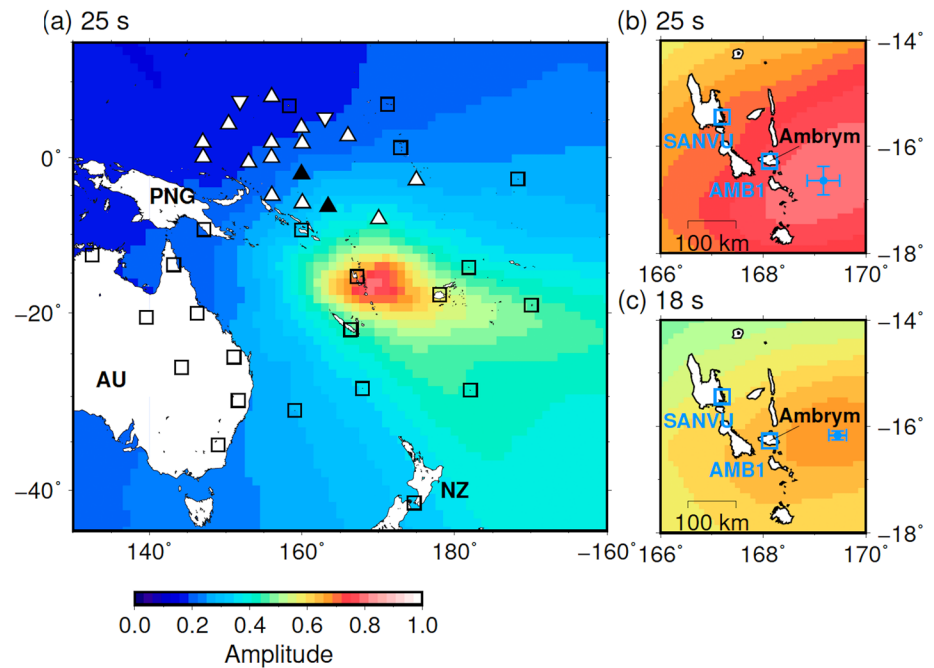


**Figure 2.** Station maps and the results of the grid-search source location. Triangles represent the stations of the OJP array (normal and inverted ones for BBOBS and island stations, respectively), and squares represent permanent land stations employed for the analysis. Two solid triangles denote OJ14 (northern) and OJ16 (southern) stations used in Figure 3c. Color contours indicate the amplitude of stacked NCFs (equation 1) normalized by the number of station pairs used for stacking. (a) The result of the grid-search source location on a  $1^\circ$  grid for the 25 s signal. (b, c) The close-up of the results of the  $0.1^\circ$  grid-search for the 25 s signal (b) and 18 s signal (c) around the Ambrym island. The blue points with error bars indicate the optimal bootstrap average location with one standard errors. Note that AMB1 is not used for the source location estimation. The color scale is common for all results.

In order to estimate the location of the signal sources, we conduct a grid search employing the NCFs similar to the previous studies (Shapiro et al., 2006). In addition to the OJP array data set, we incorporate records from regional permanent broadband seismic stations for better spatial coverage (Figure 2a). The analysis is done for data recorded from April to September 2016 when the 25 and 18 s signals have a strong amplitude (note that the data recording ended at the end of September 2016 for most of the OJP stations). We compute NCFs using 4,000-s-long sections considering the large interstation distances (6,184 km for the largest separation) and discard those whose signal-to-noise ratio is less than two; here, signal and noise levels are measured, respectively, by average Fourier amplitudes between 0.030 and 0.050 (0.050 and 0.070) Hz for the 25 (18) s signal and between 0.020 and 0.030 Hz. After band-pass filtering the NCFs with a Gaussian function centered at 0.040 (0.057) Hz, we take the envelopes of the filtered NCFs in the time domain and normalize each by its maximum value to extract arrival time information but not amplitude.

We search for a source location  $(x, y)$ , where  $x$  and  $y$  are longitude and latitude, respectively, that maximizes the stacked amplitude,  $E$ , of envelopes having the Rayleigh wave group velocity,  $U$ , as a parameter:

$$E(x, y, U) = \sum_i H_i(t_i) \quad (1)$$

where  $H_i(t_i)$  denotes the envelope amplitude for  $i$ th station pair (station  $j$  and  $k$ ) and  $t_i$  for a group travel time difference between the two stations for a given group velocity; more explicitly,  $t_i(x, y, U) = [d_j(x, y) - d_k(x, y)]/U$ , where  $d_j$  and  $d_k$  are great-circle distances connecting the station and a trial source at  $(x, y)$ .

The grid search is conducted for three parameters,  $(x, y, U)$ , first on a  $1^\circ$  grid with a 0.1 km/s step in group velocity  $U$  ranging between 3.0 and 4.3 km/s for the 25 s source and 2.8 and 3.8 km/s for the 18 s; we then use a  $0.1^\circ$  grid in  $14^\circ \times 8^\circ$  area around the estimated source, and the optimal source location and the standard

errors are estimated from 100 bootstrap samples: A bootstrap sample consists of randomly selected station pairs of the same data size as the original with duplicates allowed. Both the 25 and 18 s signal sources are estimated around the Vanuatu Arc:  $169.18^{\circ}\text{E} \pm 0.31^{\circ}$ ,  $16.65^{\circ}\text{S} \pm 0.27^{\circ}$  with a group velocity of  $3.56 \pm 0.09$  km/s for the 25 s signal (Figure 2b), and  $169.45^{\circ}\text{E} \pm 0.17^{\circ}$ ,  $16.18^{\circ}\text{S} \pm 0.09^{\circ}$  with a group velocity of  $3.09 \pm 0.03$  km/s for the 18 s signal (Figure 2c). The estimated source locations for both the 25 and 18 s signals are similar to the previous study, where Zeng and Ni (2014) located the source of their 26 s signal in the Vanuatu Arc. They calibrated the source location ( $168.5^{\circ}\text{E}$ ,  $17.5^{\circ}\text{S}$  assuming homogeneous velocity structure) using local earthquakes and relocated the source at  $167.8^{\circ}\text{E}$ ,  $16.4^{\circ}\text{S}$ , suggesting a possible connection with the activity of the Ambrym volcano. We confirm their conclusion by locating a local earthquake near the Ambrym island using our method and observing nearly  $1^{\circ}$  bias to the eastern direction (Text S1), which is consistent with their result. Here, instead of further relocating the estimated sources, we directly compare the NCFs with seismic records observed around the estimated source area to delineate the source origin. We also note that contamination of the 25 s signal by the 26 s signal originated from the Gulf of Guinea is unlikely (Zeng & Ni, 2014; Figure S1).

## 2.2. Regional and Local Observations

We investigate spectrograms recorded by stations SANVU and AMB1 located around the estimated source area (Figures 2b and 2c) and compare them with the cross-spectral density (CSD) observed at the OJP array. SANVU, a part of the GEOSCOPE network, uses a three-component broadband seismometer (STS-2), and AMB1, a part of the Vanuatu seismic network, uses a three-component intermediate-period broadband seismometer (CMG-40T). A comparison of the amplitude of distant earthquakes recorded at SANVU and AMB1 suggests that the reported instrument response of AMB1 at IRIS DMC is likely incorrect and thus re-estimated (see Figure S2 and Text S3 for the details). Spectrograms of vertical component velocity seismograms are constructed from daily power-spectral densities (PSDs) that are taken from the median of the Fourier spectra computed for 2,000-s-long sections. The CSDs are computed by the same procedure described in section 2.1 but without spectral whitening.

Strong and persistent signal peaks appear at around 25 and 18 s in the spectrograms at SANVU and AMB1 (Figures 3a and 3b) and in the spectrogram of CSDs between OJ16 and OJ14 (Figure 3c). These signals show similar amplitude variations with time, and the dominant periods are stable during the observation period. Although the observation periods do not overlap each other for AMB1 and the OJ16-OJ14 pair, time variations of their signal power are both consistent with that of SANVU. We, therefore, consider that the 25 and 18 s signals observed at the OJP array and AMB1 have the same origin. AMB1 is the closest to the signal source among these stations because the signal amplitude of AMB1 is about an order larger than the others, which cannot be explained by the site amplification effect (Figure S3). These observations strongly indicate that the 25 and 18 s signals observed by the OJP array originate from the region near the station AMB1. We consider the signals are generated by an active source rather than a passive scatterer of oceanic microseisms (Ma et al., 2013) because no significant correlation between the secondary microseism (5–10 s) and the 25 and 18 s signals are observed (Figure S4).

The station AMB1 is a part of the Vanuatu network operated by the Vanuatu Geoscience Observatory and located in the Ambrym volcanic island. Three-component seismograms at AMB1 are shown in Figure 4 for two different passbands targeting at the 25 s (0.040 Hz) and 18 s (0.057 Hz) signals. The 25 s signal is coherent between the NS and vertical components (Figure 4a), whereas the EW component whose amplitude is smaller than the NS behaves differently; the 18 s signal is coherent among three components (Figure 4b). These observations indicate that waveforms are simple enough to investigate the source origin via the polarization analysis (Figures 4c and 4d), which is conducted as follows: (1) time-windows containing earthquakes and/or glitches are discarded, and then three-component seismograms are band-pass filtered at the target frequency windows to make 200-s-long sections with a 50% overlap; (2) eigenvectors and eigenvalues of a covariance matrix are computed from NS and EW component 200 s sections, and the polarization azimuth is obtained (Jurkevics, 1988); (3) the polarization dip is computed in the same procedure but using radial and vertical component seismograms, where a radial component is computed using the polarization azimuth.

The results show that both the 25 and 18 s signals are well-polarized, indicating  $\text{N}4^{\circ}\text{W} \pm 11^{\circ}$  azimuth with  $22^{\circ} \pm 5^{\circ}$  dip and  $\text{N}16^{\circ}\text{E} \pm 4^{\circ}$  azimuth with  $17^{\circ} \pm 3^{\circ}$  dip, respectively (Figure 4e), where the means and the

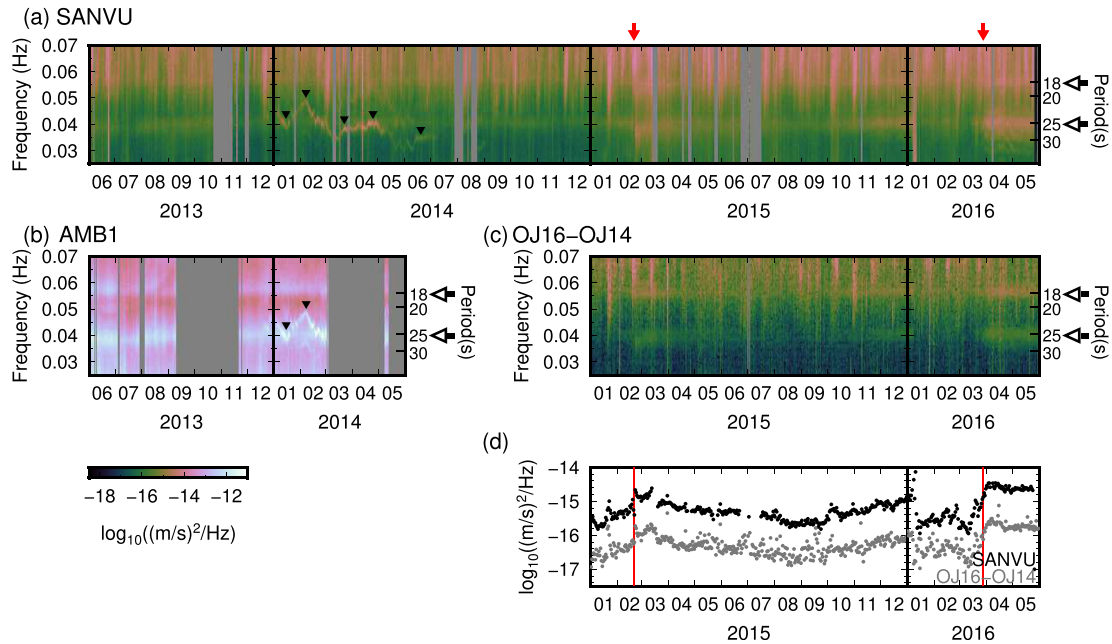


**Figure 3.** Comparison of spectrograms of the vertical component velocity seismograms. (a, b) The power-spectral density (PSD) for stations SANVU and AMB1 shown in Figure 2b. Black arrows indicate positions of 25 and 18 s. (a) For SANVU: The red arrows indicate 20 February 2015 and 28 March 2016, when signal intensifications are observed. (b) For AMB1: The black triangles show the fluctuating signal around 25 s (0.04 Hz). (c) The cross-spectral density (CSD) for the OJ16-OJ14 pair computed without spectral whitening. The color scale is common among all spectrograms. (d) A comparison of PSD and CSD for the 25 s signal (averaged in a frequency range of 0.038–0.042 Hz) for SANVU (black) and OJ16-OJ14 pair (gray). The red lines correspond to the dates of red arrows in (a).

standard deviations are obtained by fitting Gaussian functions to the histograms of all the 200 s window. Azimuths are more variable than dips for the 25 s signal, and both azimuths and dips are poorer polarized than those of the 18 s signal (Figure 4e). The fact that the polarizations are quite linear and that the polarization directions of both long-period signals point toward the area right beneath the active cones (Figure 4f) makes us to conclude that the sources of the 25 and 18 s signals are the volcanic activities of the Ambrym volcano.

### 3. Discussion

The Ambrym volcano is one of the most active volcanoes in the Vanuatu Arc. It is characterized by a 12-km-wide caldera hosting two active cones, Marum and Benbow. The volcano recently erupted in February 2015 and in December 2018 (Hamling et al., 2019; Hamling & Kilgour, 2020). The intensification of the 25 and 18 s signals is observed in the spectral densities (Figure 3d), and the one on 20 February 2015 corresponds to the intra-caldera minor eruption (Figure S5 and Hamling & Kilgour, 2020).

Legrand et al. (2005) installed a three-component broadband seismometer (STS-2) on the southwestern flank of Ambrym volcano (about 9 km from the Benbow crater) from July to November 2000 and observed persistent long-period tremors centered around 18–22 s (Figure 4f). Based on the results of the polarization analysis, they concluded that the long-period tremors originate from two sources: one in the central-to-eastern part of the caldera where the 1986 eruption took place and the other in the western part between Marum and Benbow cones. The estimated depths of the sources are between 2.7 and 2.9 km below sea level. Although they did not explicitly identify two different spectral peaks for those sources, their observation, in terms of the peak period, is generally similar to ours, except that one of the peak periods of our observation (25 s) is outside of their period range. Also, the inferred source depths and locations may be different as shown below.

The polarization analysis of the 25 and 18 s signals suggests the existence of multiple signal sources at shallow depth. The consistent time variations between the 25 and 18 s in the spectrograms (e.g., Figure 3c for March–April 2016) imply that the two sources are physically connected. Recent studies suggest the existence of

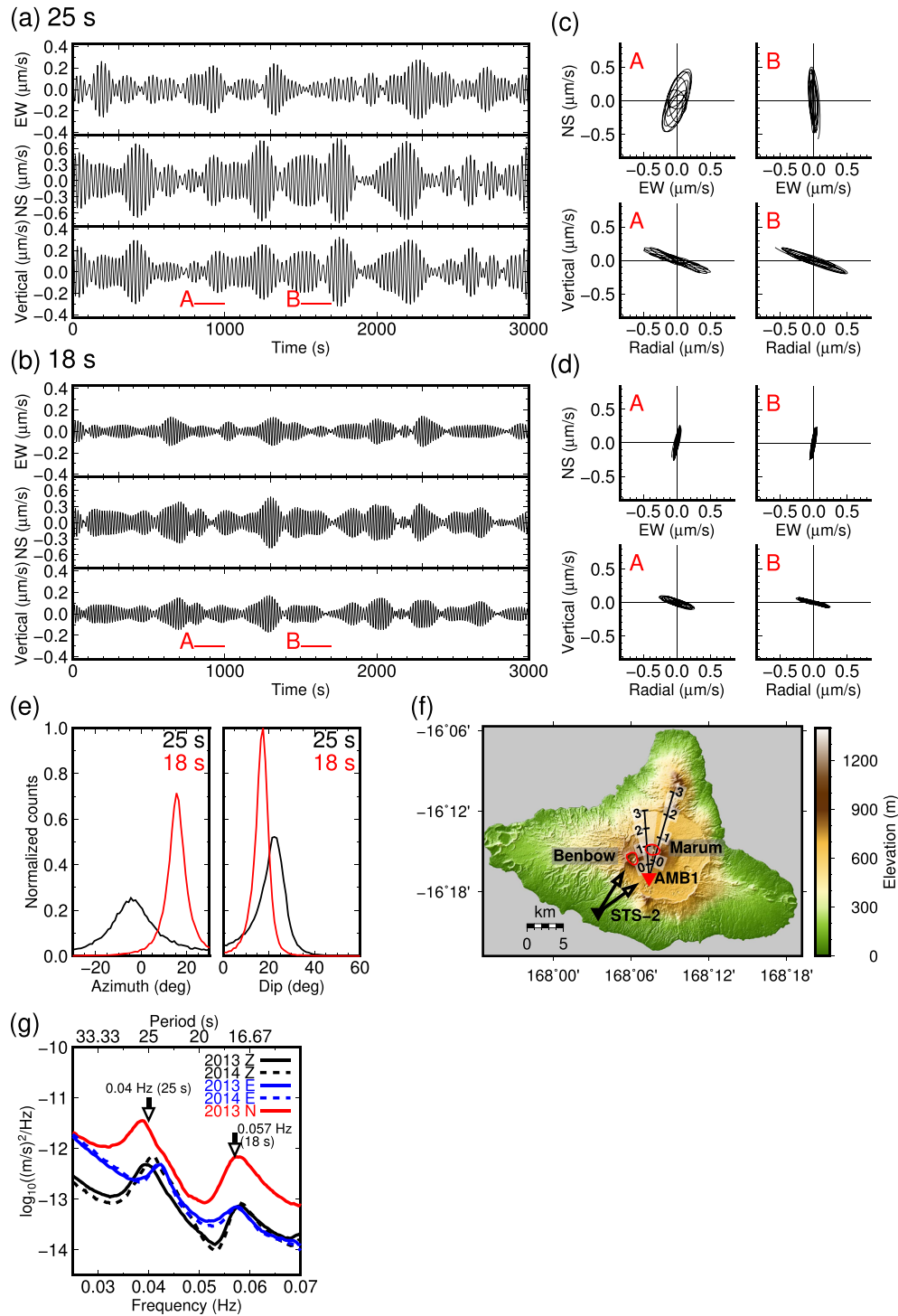


**Figure 4.** Examples of three-component seismograms at AMB1. (a, b) Fifty-minute long seismograms (start at 07:25:00 UTC 4 June 2013) band-pass filtered between 0.035 and 0.045 Hz targeting for 25 s (a) and 0.052 and 0.065 Hz for 18 s (b). The scale for the NS component is twice of the other components. (c, d) Particle motions in the horizontal (top) and vertical (bottom) plane for 200-s-long seismograms for the time windows indicated by the red lines in (a) and (b). (e) Histograms of polarization directions (azimuth: left; dip: right) for 200-s-long sections for the 25 s (red) and 18 s (black) signals recorded from June to August 2013. (f) Topography of the Ambrym volcano with station locations (red triangle for AMB1 and black for the STS-2 seismograph of Legrand et al., 2005). Black arrows at STS-2 indicate polarization azimuths estimated by Legrand et al. (2005). The two black lines represent the mean polarization azimuths of the long-period signals (with white-shaded areas for one standard deviation ranges) estimated in this study. The numbers along the black lines with ticks indicate the projected source depths below the sea level if the source is there. Red circles show rims of Benbow and Marum cones. (g) A comparison of yearly power-spectral densities of three components of AMB1. Black arrows indicate the position of 0.04 and 0.057 Hz.

multiple magma reservoirs beneath the two active cones at depth  $\sim 1\text{--}5$  km below the sea level (e.g., Hamling et al., 2019). Considering that the wavelengths of the long-period tremors ( $> \sim 60$  km) are much larger than the distance between the active cones and the station ( $< 5$  km), AMB1 is likely located within the near-field range from the source (e.g., Aki & Richards, 2002). Near-field seismic records contain various types of waves including static displacement, the near-field terms, and  $P$  and  $S$  waves. If the source is dominated by the isotropic component, as often the case for volcanic volumetric sources, the polarization of filtered seismograms is rectilinear and points to the source centroid (Legrand et al., 2000). Then, we can estimate the source locations using the estimated polarization directions as done in Aso (e.g., Kawakatsu et al., 2000; Kawakatsu & Yamamoto, 2015; Legrand et al., 2000) and in Ambrym (Legrand et al., 2005).

As we have only one observation point here, the best we can do is to infer the range of source locations for presumed depths; Figure 4f shows the inferred source locations assuming variable source depths or vice versa. If we assume the signal sources are located beneath Marum, the source depth is  $\sim 0\text{--}1$  km below the sea level for both 25 and 18 s signals, indicating that they are more likely to be associated with the activity of the shallow magma system at depths of 1–2 km (Hamling et al., 2019). As like the case of the Aso volcano in Japan, they could be due to vibrations of conduits connecting the magma system to the surface cones, possibly sustained by the hydrothermal reaction at the aquifer. Considering the long-period nature of signals, temporal deployment of broadband seismometers in the island should allow determining the source geometry better (Yamamoto et al., 1999).

The spectral width of two signals are similar, but the 25 s signal shows more variable peak frequencies than that of the 18 s signal (Figure 4g). The polarization azimuths of the 25 s signal are more variable than those of the 18 s signal (Figure 4e). This might suggest that the source for the 25 s signal is distributed wider in the lateral direction compared to that of the 18 s signal; it may be related to a subsurface conduit system that connects Marum and Benbow cones or the dykes below the cones recently imaged by the analysis of the ALOS-2 InSAR data for the 2015 eruption (Hamling & Kilgour, 2020). From January to June 2014, spectrograms show signals whose peak periods are time-variant and fluctuate around 33 s (0.03 Hz), 25 s (0.04 Hz), and 20 s (0.05 Hz); those signals show a similar time variation, and the one that fluctuates around 25 s is the strongest (Figures 3a and 3b). These may be related to the change of the magmatic fracture system prior or posterior to the eruptions.

#### 4. Conclusions

Ambient noise cross-correlation functions observed by the OJP array in the western-central Pacific indicate the existence of spatially localized signal sources that generate long-period seismic waves at periods around 25 and 18 s. The sources are determined in the Vanuatu Arc where the Ambrym volcano exists that generates the long-period seismic waves whose amplitude variations are consistent with the array observation. Polarization analysis of local seismic records in the Ambrym volcano suggests the existence of multiple sources possibly located at depths of  $\sim 0\text{--}1$  km from the sea surface beneath the active cones. This work demonstrates a potential usage of a BBOBS array to discover unknown long-period persistent seismic sources (possible beneath the ocean) via the ambient noise cross-correlation function analysis, and this may, in turn, help our better understanding of the ambient noise seismic field for future structural or monitoring studies.

#### Data Availability Statement

OJP array data will become available online (<http://p21.jamstec.go.jp/top/> and <http://ohpdm.eri.u-tokyo.ac.jp>) after the moratorium period. Poles and zeroes of CMG-40T used at AMB1 are referenced from the website ([https://ds.iris.edu/NRL/sensors/guralp/guralp\\_cmg40t\\_sensors.html](https://ds.iris.edu/NRL/sensors/guralp/guralp_cmg40t_sensors.html)). GMT (Wessel et al., 2013) and SAC2000 (Goldstein & Snoke, 2005) are used in this study.

#### References

- Aki, K., & Richards, P. G. (2002). *Quantitative Seismology* (2nd ed.). Sausalito, California: University Science Books.
- Bell, S. W., Forsyth, D. W., & Ruan, Y. (2015). Removing noise from the vertical component records of ocean-bottom seismometers: Results from year one of the Cascadia Initiative. *Bulletin of the Seismological Society of America*, *105*(1), 300–313. <https://doi.org/10.1785/0120140054>

#### Acknowledgments

We thank the captains and crews of R/V MIRAI of JAMSTEC and R/V HAKUHO-MARU of JAMSTEC for the deployment and recovery cruises. We also acknowledge the work of those who operate ANSN, GEOSCOPE (<https://doi.org/10.18715/GEOSCOPE>), IRIS/IDA (<https://doi.org/10.7914/SN/II>), IRIS/USGS (<https://doi.org/10.7914/SN/IU>), Pacific 21, and Vanuatu Seismic Network. IRIS DMC and OHP DMC provided access to the seismic data used in this study. Y.K. thanks Kiwamu Nishida for his valuable discussion. We also thank reviewers and the associate editor for comments that improved the manuscript. This work is partly supported by JSPS KAKENHI Grant Numbers JP15H03720, JP18H03735, and JP20J11260.

- Bensen, G. D., Ritzwoller, M. H., Barmin, M. P., Levshin, A. L., Lin, F., Moschetti, M. P., et al. (2007). Processing seismic ambient noise data to obtain reliable broad-band surface wave dispersion measurements. *Geophysical Journal International*, *169*(3), 1239–1260. <https://doi.org/10.1111/j.1365-246X.2007.03374.x>
- Crawford, W., & Webb, S. (2000). Identifying and removing tilt noise from low-frequency (< 0.1 Hz) seafloor vertical seismic data. *Bulletin of the Seismological Society of America*, *90*(4), 952–963. <https://doi.org/10.1785/0119990121>
- Goldstein, P., & Snoke, A. (2005). SAC Availability for the IRIS Community. *DMS Electronic Newsletter*, *7*(1), Feature Article, New York.
- Hamling, I. J., Cevuar, S., & Garaebiti, E. (2019). Large-scale drainage of a complex magmatic system: Observations from the 2018 eruption of Ambrym volcano, Vanuatu. *Geophysical Research Letters*, *46*, 4609–4617. <https://doi.org/10.1029/2019GL082606>
- Hamling, I. J., & Kilgour, G. (2020). Goldilocks conditions required for earthquakes to trigger basaltic eruptions: Evidence from the 2015 Ambrym eruption. *Science Advances*, *6*, eaaz5261. <https://doi.org/10.1126/sciadv.aaz5261>
- Holcomb, L. G. (1980). Microseisms: A twenty-six-second spectral line in long-period earth motion. *Bulletin of the Seismological Society of America*, *70*(4), 1055–1070.
- Holcomb, L. G. (1998). Spectral structure in the earth's microseismic background between 20 and 40 seconds. *Bulletin of the Seismological Society of America*, *88*(3), 744–757.
- Jurkevics, A. (1988). Polarization analysis of three-component array data. *Bulletin of the Seismological Society of America*, *78*(5), 1725–1743.
- Kaneshima, S., Kawakatsu, H., Matsubayashi, H., Sudo, Y., Tsutsui, T., Ohminato, T., et al. (1996). Mechanism of phreatic eruptions at Aso volcano inferred from near-field broadband seismic observations. *Science*, *273*(5275), 642–645. <http://doi.org/10.1126/science.273.5275.642>
- Kawakatsu, H., Kaneshima, S., Matsubayashi, H., Ohminato, T., Sudo, Y., Tsutsui, T., et al. (2000). Aso94: Aso seismic observation with broadband instruments. *Journal of Volcanology and Geothermal Research*, *101*(1–2), 129–154. [https://doi.org/10.1016/S0377-0273\(00\)00166-9](https://doi.org/10.1016/S0377-0273(00)00166-9)
- Kawakatsu, H., Ohminato, T., & Ito, H. (1994). 10s-period volcanic tremors observed over a wide area in southwestern Japan. *Geophysical Research Letters*, *21*(18), 1963–1966. <https://doi.org/10.1029/94GL01683>
- Kawakatsu, H., & Yamamoto, M. (2015). 4.15—Volcano seismology. In G. Schubert (Ed.), *Treatise on Geophysics* (2nd ed., pp. 389–419). Oxford: Elsevier. <https://doi.org/10.1016/B978-0-444-53802-4.00081-6>
- Kawano, Y., Isse, T., Takeo, A., Kawakatsu, H., Suetsugu, D., Shiobara, H., et al. (2019). Array analysis of OBS recordings at Ontong Java Plateau: Preliminary analysis via seismic interferometry, Abstract [D113C-0023] presented at 2019 Fall Meeting, AGU, San Francisco, CA, 9–13 Dec.
- Légrand, D., Kaneshima, S., & Kawakatsu, H. (2000). Moment tensor analysis of near-field broadband waveforms observed at Aso volcano, Japan. *Journal of Volcanology and Geothermal Research*, *101*(1–2), 155–169. [https://doi.org/10.1016/S0377-0273\(00\)00167-0](https://doi.org/10.1016/S0377-0273(00)00167-0)
- Légrand, D., Rouland, D., Frogneux, M., Carniel, R., Charley, D., Roult, G., & Robin, C. (2005). Interpretation of very long period tremors at Ambrym volcano, Vanuatu, as quasi-static displacement field related to two distinct magmatic sources. *Geophysical Research Letters*, *32*, L06314. <https://doi.org/10.1029/2004GL021968>
- Ma, Y., Clayton, R. W., Tsai, V. C., & Zhan, Z. (2013). Locating a scatterer in the active volcanic area of Southern Peru from ambient noise cross-correlation. *Geophysical Journal International*, *192*(3), 1332–1341. <https://doi.org/10.1093/gji/ggs103>
- Nishida, K., Kawakatsu, H., & Obara, K. (2008). Three-dimensional crustal S wave velocity structure in Japan using microseismic data recorded by Hi-net tiltmeters. *Journal of Geophysical Research*, *113*, B10302. <https://doi.org/10.1029/2007JB005395>
- Oliver, J. (1962). A worldwide storm of microseisms with periods of about 27 seconds. *Bulletin of the Seismological Society of America*, *52*(3), 507–517.
- Oliver, J. (1963). Additional evidence relating to “a worldwide storm of microseisms with periods of about 27 seconds”. *Bulletin of the Seismological Society of America*, *53*(3), 681–685.
- Shapiro, N. M., Campillo, M., Stehly, L., & Ritzwoller, M. H. (2005). High-resolution surface-wave tomography from ambient seismic noise. *Science*, *307*(5715), 1615–1618. <https://doi.org/10.1126/science.1108339>
- Shapiro, N. M., Ritzwoller, M. H., & Bensen, G. D. (2006). Source location of the 26 sec microseism from cross-correlations of ambient seismic noise. *Geophysical Research Letters*, *33*, L18310. <https://doi.org/10.1029/2006GL027010>
- Suetsugu, D., Shiobara, H., Sugioka, H., Tada, N., Ito, A., Isse, T., et al. (2018). The OJP array: Seismological and electromagnetic observation on seafloor and islands in the Ontong Java Plateau. *JAMSTEC-R*, *26*, 54–64. <https://doi.org/10.5918/jamstecr.26.54>
- Takeo, A., Nishida, K., Isse, T., Kawakatsu, H., Shiobara, H., Sugioka, H., & Kanazawa, T. (2013). Radially anisotropic structure beneath the Shikoku Basin from broadband surface wave analysis of ocean bottom seismometer records. *Journal of Geophysical Research: Solid Earth*, *118*(6), 2878–2892. <https://doi.org/10.1002/jgrb.50219>
- Wessel, P., Smith, W. H., Scharroo, R., Luis, J., & Wobbe, F. (2013). Generic mapping tools: Improved version released. *Eos, Transactions American Geophysical Union*, *94*(45), 409–410. <https://doi.org/10.1002/2013EO450001>
- Xia, Y., & Chen, X. (2020). Observation of a new long-period (16-s) persistent tremor originating in the Gulf of Guinea. *Geophysical Research Letters*, *47*, e2020GL088137. <https://doi.org/10.1029/2020GL088137>
- Xia, Y., Ni, S., & Zeng, X. (2013). Twin enigmatic microseismic sources in the Gulf of Guinea observed on intercontinental seismic stations. *Geophysical Journal International*, *194*, 362–366. <https://doi.org/10.1093/gji/ggt076>
- Yamamoto, M., Kawakatsu, H., Kaneshima, S., Mori, T., Tsutsui, T., Sudo, Y., & Morita, Y. (1999). Detection of a crack-like conduit beneath the active crater at Aso volcano Japan. *Geophysical Research Letters*, *26*(24), 3677–3680. <https://doi.org/10.1029/1999GL005395>
- Zeng, X., & Ni, S. (2010). A persistent localized microseismic source near the Kyushu Island, Japan. *Geophysical Research Letters*, *37*, L24307. <https://doi.org/10.1029/2010GL045774>
- Zeng, X., & Ni, S. (2011). Correction to “A persistent localized microseismic source near the Kyushu Island, Japan”. *Geophysical Research Letters*, *38*, L16320. <https://doi.org/10.1029/2011GL048822>
- Zeng, X., & Ni, S. (2014). Evidence for an independent 26-s microseismic source near the Vanuatu islands. *Pure and Applied Geophysics*, *171*, 2155–2163. <https://doi.org/10.1007/s00024-014-0811-1>

## Reference From the Supporting Information

- Peterson, J. R. (1993). Observations and modeling of seismic background noise. U.S. Geological Survey. Open-File Reports., 93-322. <https://doi.org/10.3133/ofr93322>